A LEED study of MgO(100). I. Experiment

1974 J. Phys. C: Solid State Phys. 7 4236

(http://iopscience.iop.org/0022-3719/7/23/010)

J. Phys: C: Solid State Phys., Vol. 7, 1974. Printed in Great Britain.

A LEED study of MgO(100): I. Experiment

K O Legg†, M Prutton and C Kinniburgh
Department of Physics, University of York, Heslington, York

Received 17 July 1974

Abstract. Normalized LEED intensity–voltage data have been obtained for the (100) surface of MgO prepared by cleavage *in-situ*. Corrections for the variation of primary current with energy and for varying optical attentuation of the grids as beams move across the screen have both been applied. Variations in surface potential with primary energy have been estimated using the position of the $L_{2,3}VV$ peak in the Auger spectrum. Data are given for four beams at normal incidence, the specular beam in two azimuths and at angles of incidence of 5, 10, 15 and 20° and the (10) beams at one azimuth and the same angles of incidence.

1. Introduction

Considerable progress has been made during the last few years towards agreement of experimental and theoretical intensity against energy curves obtained by low-energy electron diffraction from low index faces of metals (eg Jepsen *et al* 1972). This success has encouraged the study of the structure of ordered adlayers using LEED (eg Andersson and Pendry 1972, 1973, Demuth *et al* 1973). However, little work has been reported on LEED data from the surfaces of compounds. Data obtained by McRae and Caldwell (1967) for the LiF(100) surface have been analysed by Laramore and Switendick (1972) who conclude that some features in the LEED spectra show evidence of the surface rumpling of (100) alkali halide surfaces predicted by Benson and Claxton (1968). The difficulty with alkali halides as subjects of study using LEED is that the incident electrons cause preferential desorption of the halogen leaving the surface metal-rich (Gallon *et al* 1970, Palmberg *et al* 1968). Although McRae and Caldwell's LEED data were obtained at 300 °C, at which temperature halogen ions presumably diffuse out of the bulk to replace those lost by electron beam stimulated desorption, the composition and structure of the (100) surface must be uncertain because of this electron beam damage.

Magnesium oxide is readily available in single crystal form, can be cleaved to expose a (100) plane and is not damaged by the incident electron beam. This paper reports measurements of the LEED spectra from this material and their normalization to produce curves of reflectivity in each beam as a function of primary electron energy. A subsequent paper (II) will discuss the application to a full dynamical calculation to MgO(100) and a comparison of the normalized experimental data with theory.

† Present address: Department of Materials Science, State University of New York, Stony Brook, New York, 11794, USA.

2. Experimental

A UHV system described previously (Lord and Gallon 1973) was adapted for measuring LEED $I(V)$ curves. The system was already equipped with Varian 4 grid LEED optics and with facilities for RHEED at 15 keV, for Auger electron spectroscopy and for quadrupole mass spectrometry. The system was modified to provide *in-situ* cleavage of the MgO crystal, and semi-automatic data collection was incorporated using a commercial photometer (Pritchard-Spectra-Physics Inc.) and a data transfer unit to punch the information onto paper tape.

Two normalization factors were taken into account in changing measured intensities into reflectivities with respect to the incident beam current. A correction was made for the variation of incident current with energy (Jona 1970) by biassing the sample negatively to reflect the primary beam back onto the fluorescent screen where the collected current was measured. This gave the incident beam current reduced by the electron transparency of the four grids (about 80% each). The second correction, which is not conventionally applied to LEED data, corrects for the variation of the optical transparency of the grids with the direction of observation of a LEED spot. This transparency varies from about $(0{\cdot}8)^4$ along the electron optical axis to zero when the light emitted from the fluorescent screen strikes the grids near grazing incidence (figure 1). For a rough phosphor surface emitting

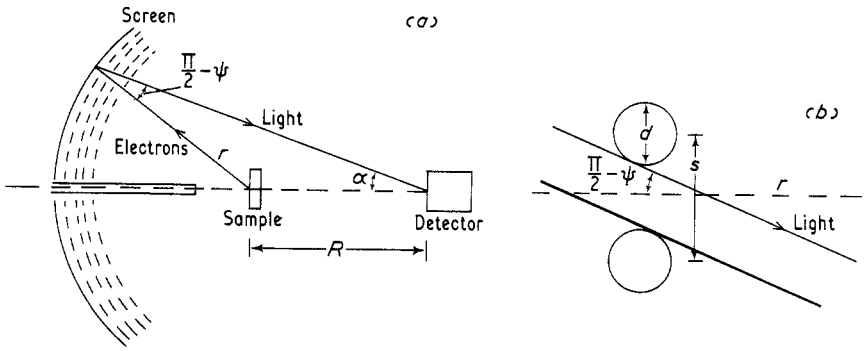

Figure 1. (*a*) Geometry of the photometer arrangement. (*b*) Definition of the symbols used to derive the attenuation of the spot brightness by the presence of the grid bars of diameter d.

light with a cosine intensity distribution through four grids it can be shown that the ratio T_α of the measured spot intensity I_{MEAS} to the actual spot intensity I_S on the fluorescent screen is given approximately by:

$$T_\alpha = \frac{I_{\mathrm{MEAS}}}{I_S} = t_\alpha^4 \left(1 - \frac{d}{s}\right)^4 \sin\psi, \tag{1}$$

where

$$t_\alpha = 1 - \frac{d}{s[1 - (R/r)^2 \sin^2\alpha]^{1/2}}. \tag{2}$$

Instead of applying a calculated correction to the measured intensities the optical function T_α was measured by biassing the sample negatively to throw the primary beam back onto the screen. This spot was moved about with an external magnet and the current flowing from the screen, the spot intensity and the photometer angle α all measured for a variety of spot positions. The measured spot intensity per unit current was then plotted

against α and could be compared with equation (1). In the derivation of equation (1) it is assumed that the current flowing from the screen is due entirely to electrons in the spot and not to those which have been diffusely scattered on passing through the grids. The variation with electron trajectory of the focussing properties of the grids has been neglected.

In order to apply the two corrections described above, and also to help comparison with theory, the data were collected in digital form and corrections applied afterwards in a digital computer. The system was arranged to change the primary energy in discrete steps and to sample the energy, the spot intensity and the photometer orientation at each step. A diagram of the overall system is shown in figure 2. The operator started the energy

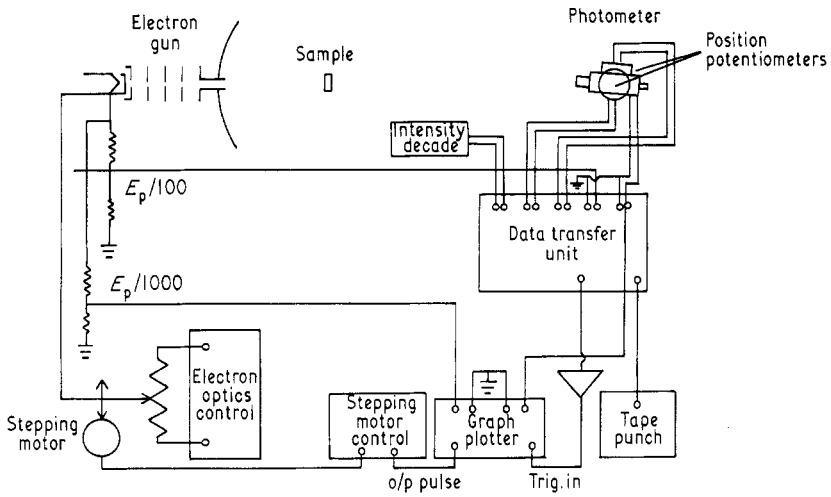

Figure 2. Block diagram of the data collection system.

scan and then controlled the photometer manually to track the moving diffraction spot whilst potentiometers gave continuously varying potentials which could be related to the angle α.

The sample holder was designed to hold crystals up to 1 cm $\times$ 1 cm in cross section contained within a copper tube which could be heated to 500 °C and cooled to -150 °C and rotated about its axis to provide azimuthal rotations ϕ of $\pm 85°$. In addition the sample could be translated horizontally and vertically, tilted $\pm 3°$ about a horizontal axis in its surface and rotated $\pm 90°$ about a vertical axis in its surface. This latter rotation gave the range of angles of incidence θ which were accessible. A stainless steel table could be brought up to support the crystal while a tool steel blade was struck so as to cleave the crystal along a (100) plane.

The angles θ and ϕ were measured by using the symmetry of the LEED $I(V)$ curves in the manner described by Jona (1970). The azimuthal axis was set to $\pm 0{\cdot}5°$ by ensuring that a relevant set of spots lay in a horizontal line determined by rotating the sample about a vertical axis in its surface and changing ϕ until all spots of the set passed through the photometer aperture (which was set at 20′ of arc). Normal incidence was found to $\pm 0{\cdot}5°$ by tilting the sample about the two axes in its surface until $I(V)$ curves for symmetrically related spots were as nearly identical as possible. Having so defined normal incidence the accuracy in θ was $\pm 0{\cdot}7°$.

The MgO crystals used were 8 mm $\times$ 8 mm $\times$ 2 cm in size already cleaved along (100)

faces. They were 99·9% pure, the principal impurities being CaO 800 ppm, Al_2O_3 100 ppm, and Fe_2O_3 100 ppm†. Samples about 8 mm × 8 mm × 4 mm were gold plated on all faces before insertion in the LEED system in order to improve electrical contact to the sample holder. After cleavage the sample thickness was 2 or 3 mm. This procedure helped to reduce the charging effects described later.

The MgO was cleaved at room temperature and a pressure of 5×10^{-10} Torr. This pressure was maintained throughout the observations.

Magnetic fields were compensated by a set of field coils around the chamber. After compensation the residual field was inhomogeneous but no greater than 15 mG anywhere within the diffraction volume. The (00) spot did not move for energies above 100 eV, below which charging set in.

3. Results

3.1. Normalization

The variation of primary current with energy, measured before and after collecting LEED data, was found to be very similar to that described by Jona (1970), falling from about 10 μA at 200 eV to 1 μA at 50 eV.

The variation of spot intensity per unit current against photometer orientation α is shown in figure 3 where the observations are compared with a curve calculated using

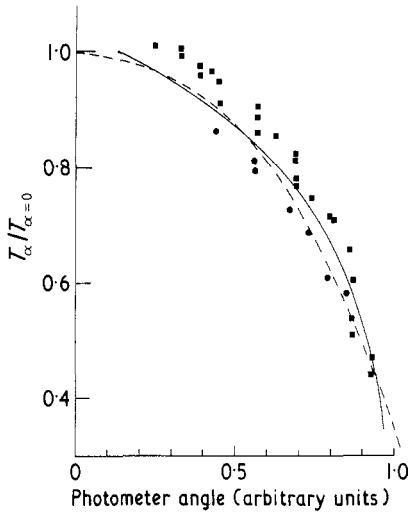

Figure 3. Screen normalization data. The circles are points on the right-hand side of the screen and the squares points on the left-hand side. The full line is the rough average used as a normalization curve. The broken line corresponds to equation (1). The ordinate is T_α divided by the value of T_α evaluated at $\alpha = 0$.

equation (1) and fitted at one point to the mean of the experimental points. It can be seen that at low energies and normal incidence, where low index diffracted beams reach the edge of the fluorescent screen, the measured intensity is down on that near the screen centre by a factor 2·5. The agreement between the observations and the curve drawn using

† Supplied by Messrs W and C Spicer Ltd.

equation (1) is taken to give support for the assumptions made in obtaining the function T_α experimentally.

The importance of these two corrections is shown in figure 4 where it can be seen that for spots near the screen edge, the screen normalization is of comparable importance to the incident current normalization. The two corrections are multiplicative and have a large effect at low energies.

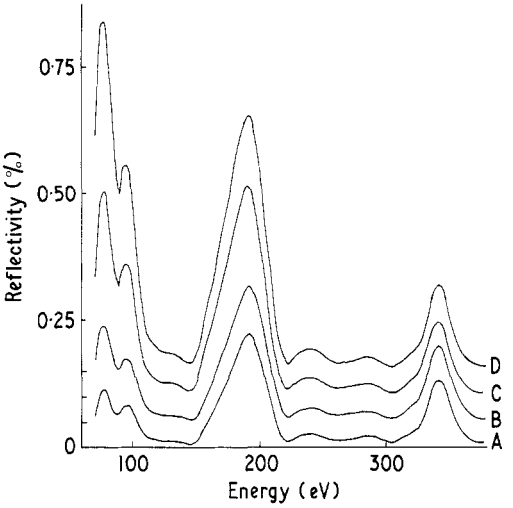

Figure 4. The effects of normalization. $I_{20}(V)$; $\theta = 15°$, $\phi = 135°$. A, raw data; B, screen correction only; C, beam current correction only; D, fully normalized.

3.2. Auger electron spectra

Auger spectra were taken before and after recording the LEED $I(V)$ curves. There was no detectable change in the spectra between these two times. The spectrum below 1 000 eV taken at the end of the run is shown in figure 5. There are very tiny traces of C, S and Cl, probably below the 0·1 monolayer level. The spectrum below 250 eV is very complex but all the peaks have been assigned to Auger processes in clean MgO and to diffraction of true secondary electrons as they emerge from clean MgO. The assignments and the interpretation of this spectrum are discussed by Janssen *et al* (1974).

The largest peak in the spectrum occurs at 24 eV and is assigned to an $L_{2,3}VV$ process in MgO. The position of this peak can be used to determine a value for the potential at the surface of the MgO. Because this material has such a high secondary electron yield—approximately 24 (Whetton and Laponsky 1957)—it comes to equilibrium with a space-charge cloud just outside its surface with the potential of the surface itself positive with respect to the grounded sample holder. Thus, Auger electrons generated at the surface are retarded before reaching the first (grounded) grid of the analysing electron optics. By comparing the position of the $L_{2,3}VV$ peak in a very thin layer of polycrystalline MgO upon grounded Mg metal with the observed position of the same peak from bulk MgO Janssen *et al* (1974) have been able to determine the size of this potential. This comparison is reasonable because the thin film of MgO cannot support a large electric field through its thickness. The $L_{2,3}VV$ peak in the thin film of MgO at ground potential was found to occur at 34 eV. It is concluded therefore that the surface of the bulk MgO crystal is at about + 10 V with respect to ground during the Auger experi-

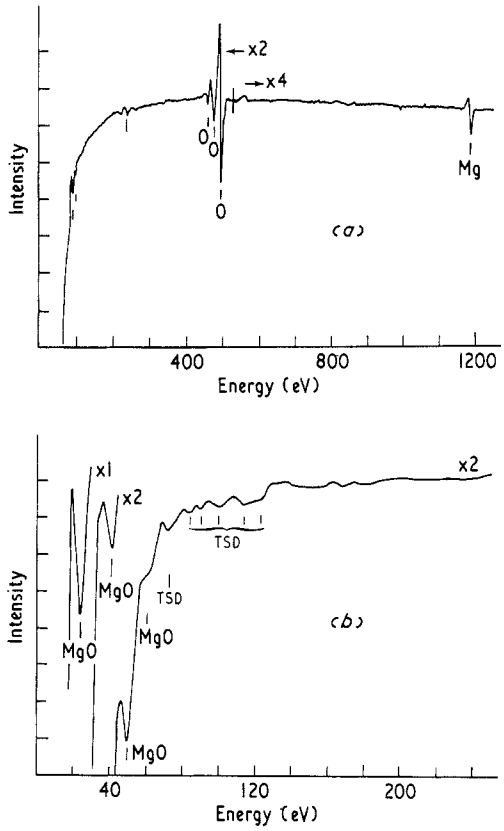

Figure 5. Auger spectra of the MgO surface after collection of the LEED data. Primary beam current approximately 3 μA; area sampled approximately 1 mm^2. (*a*) E_p = 1800 eV; modulation 5 V peak to peak; 1 s time constant. (*b*) E_p = 1000 eV; modulation 4 V peak to peak; 5 s time constant. TSD stands for true secondary generation followed by diffraction—see text.

ment. Because the $L_{2,3}$ level in the MgO is only at 55 eV it is possible to observe the position of the $L_{2,3}VV$ peak as a function of primary energy over the range used to obtain the LEED data. It was found that between 250 eV and 90 eV the $L_{2,3}VV$ feature moved from 24·5 eV to 30·5 eV as indicated in figure 6. Thus it is concluded that the surface potential changed from 9·5 eV at 250 eV to 3·5 eV at 90 eV. The surface charged negatively below 80 eV presumably because the secondary electron yield falls below unity at this primary energy.

3.3. LEED spectra

I(V) data were taken at room temperature between energies of approximately 300 eV and 90 eV. At this lower limit the first sign of movement of the spots due to unstable surface charging could be detected. Below about 60 eV the LEED pattern had vanished, presumably because the secondary electron yield of the MgO had dropped below unity and the surface had charged to $-V_p$. The primary electrons are then repelled by the sample and reach the screen without being diffracted by the crystal potential.

The convention used to label the LEED spots is indicated in figure 7. Data taken at

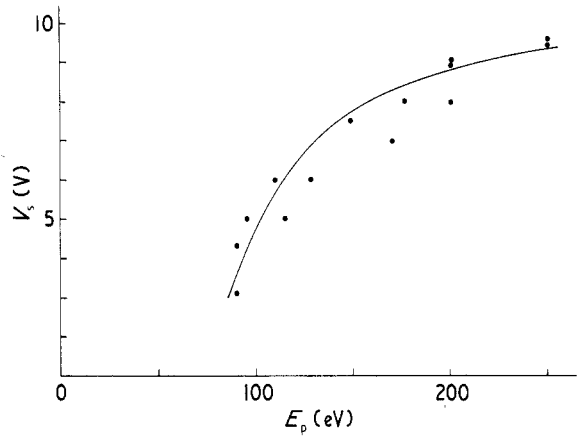

Figure 6. MgO surface potential against primary energy as derived from the shifting position of the $L_{2,3}VV$ Auger peak. The points are experimental data and the full line is drawn using $V_S = 10{\cdot}2 - (5{\cdot}3 \times 10^4/E_p^2)$.

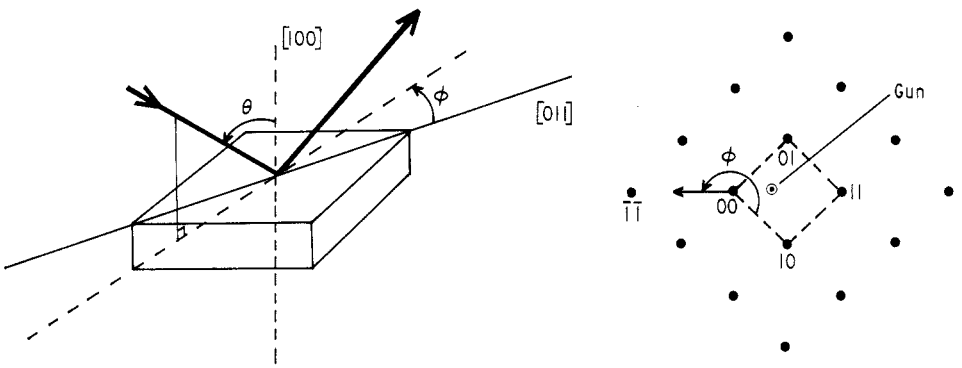

Figure 7. Definition of diffraction geometry and the convention for labelling LEED spots. The azimuthal angle ϕ is defined as the angle between the (10) direction and the direction of $k_{0\parallel}$ in the sense shown. In the example drawn above $\phi = 135°$.

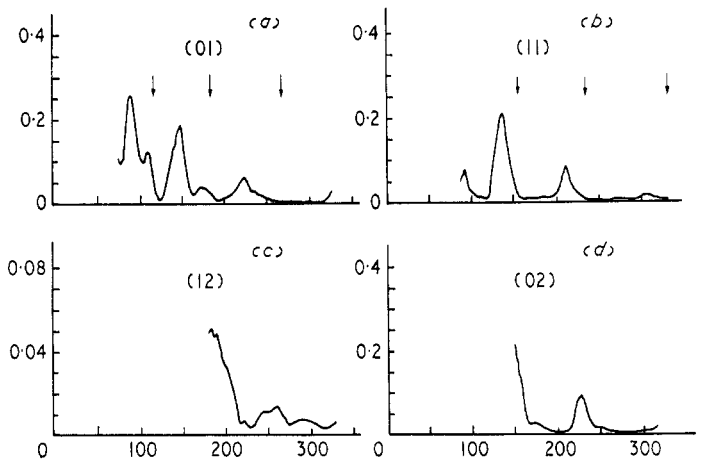

Figure 8. Diffraction data for beams at normal incidence.

Table 1. Diffraction geometries and beams used for $I(V)$ data.

ϕ	$\theta =$	$+20°$		$+15°$		$+10°$		$+5°$		$0°$	
180°		00	$\bar{1}0$	00	$1\bar{1}$	00	$0\bar{1}$	00	$0\bar{1}$	01	11
		$1\bar{1}$	$\bar{2}\bar{2}$	$1\bar{2}$	$0\bar{1}$	$\bar{1}0$	$1\bar{1}$	$\bar{1}0$	$1\bar{1}$	12	02
		$3\bar{1}$		$3\bar{1}$		20		$\bar{1}1$	20		
135°		00	10	00	10	00	10	$\bar{1}1$		01	11
		21	$2\bar{1}$	$\bar{1}1$	20	$\bar{1}0$	$\bar{1}1$			12	02
		22	20	21	$2\bar{1}$	20	21				
				22		$2\bar{1}$	22				
45°								00	01	01	11
								$0\bar{1}$	11	12	02
								$\bar{1}\bar{1}$			

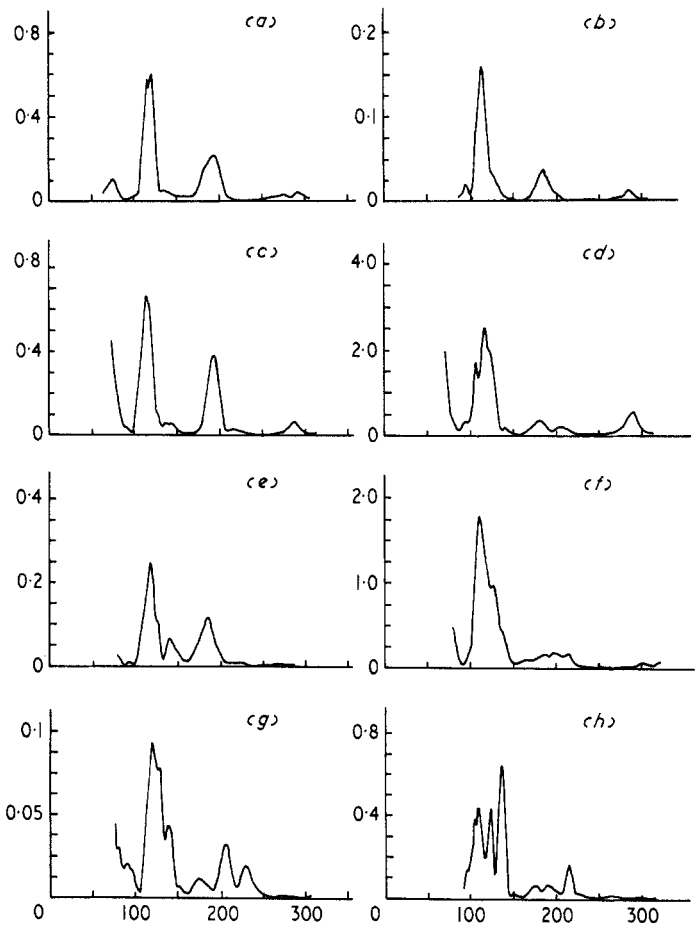

Figure 9. Diffraction data for the specular beam for three simple azimuths and for four angles of incidence θ. (*a*) $\theta = 5, \phi = 180$; (*b*) $\theta = 5, \phi = 45$; (*c*) $\theta = 10, \phi = 180$; (*d*) $\theta = 10, \phi = 135$; (*e*) $\theta = 15$; $\phi = 180$; (*f*) $\theta = 15$, $\phi = 135$; (*g*) $\theta = 20$, $\phi = 180$; (*h*) $\theta = 20$, $\phi = 135$.

normal incidence are particularly useful for first comparisons with theory because the high symmetry of this geometry can be exploited in the calculations such that a greater number of non-equivalent beams can be included for the same computation time. The data for (01), (11), (12) and (02) spots are shown in figure 8. The beam current and screen corrections have been applied to the intensity but the surface potential correction of figure 6 has *not* been applied to the energy scale. The arrows indicate the expected positions of kinematical peaks calculated using no inner potential correction and a bulk lattice constant of 4·20 Å.

Data were taken for all the spots listed in table 1†. The $I(V)$ curves for the specular beam are given in figure 9 for three simple azimuths in several angles of incidence. Similar data for (10) type beams are shown in figure 10. The curves are normalized but their energy scales are *not* corrected for charging.

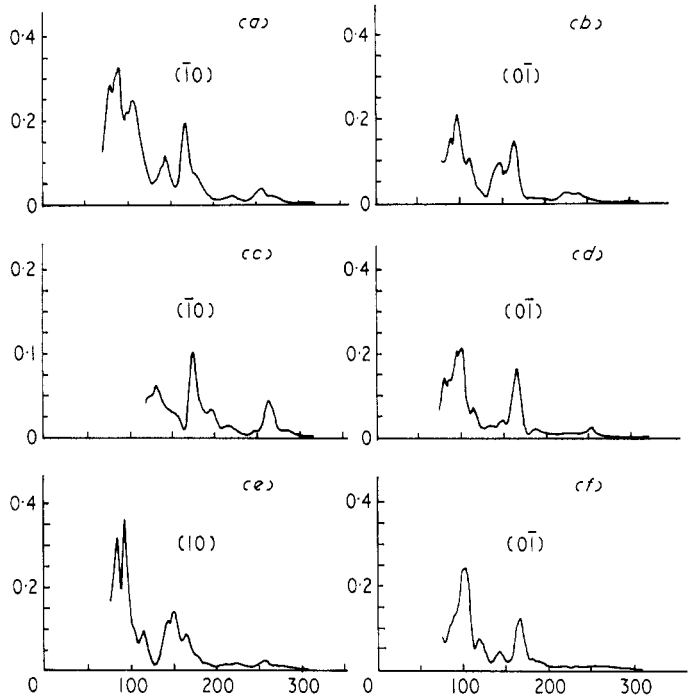

Figure 10. Diffraction data for some {01} beams for $\phi = 180°$. Note that 10(*e*) is not the same sequence as 10(*a*) and 10(*c*). (*a*) $\theta = 5$, $\phi = 180$; (*b*) $\theta = 5$, $\phi = 180$; (*c*) $\theta = 10$, $\phi = 180$; (*d*) $\theta = 10$, $\phi = 180$; (*e*) $\theta = 20$, $\phi = 180$; (*f*) $\theta = 15$, $\phi = 180$.

3.4. Surface topography

After taking the LEED spectra and making a final examination of the MgO surface by Auger spectroscopy the crystal was removed from the UHV chamber. A shadowed carbon–platinum replica was made of the surface and this was examined by transmission electron microscopy. The region used to obtain the LEED spectra showed flat terraces separated by cleavage steps at least 5 μm apart.

† These data are too extensive to reproduce here. Copies of the data are available from the authors.

3.5. Reproducibility

LEED spectra have been taken from three different MgO (100) surfaces. Only one set was carefully normalized as described above. The agreement in shape was very good, as is demonstrated by data for a (10) type beam shown in figure 11.

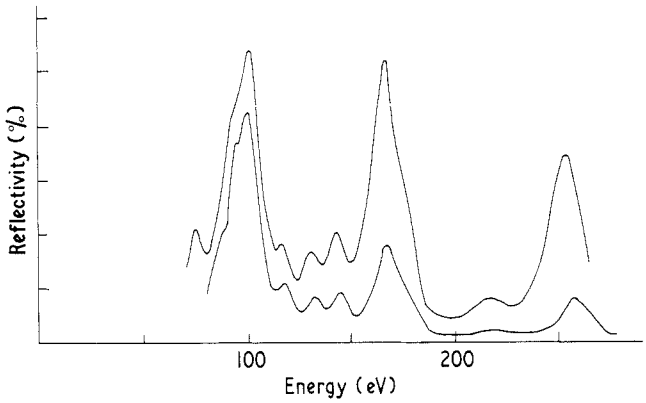

Figure 11. The reproducibility of diffraction data for the (10) beam at $\theta = 10°$ and $\phi = 135°$ for two different MgO(100) surfaces. The upper curve is unnormalized. The lower curve is fully normalized.

4. Discussion

If the energy scale is corrected by the surface potential shown in figure 6 then values for the inner potential V_{or} can be derived by subtracting the observed peak positions from the kinematically calculated positions. This has been done for 56 peaks. The values of V_{or} so derived vary from 10 eV to 57 eV. There is no clear systematic variation of V_{or} with primary energy or with θ and ϕ. The mean value of V_{or} is 23·3 eV with a standard deviation of 12 eV. The largest values of V_{or} tend to occur at the highest energies and the largest incidence have values of 20, 24 and 34 eV for 117, 119, and 1,1, 11 reflections and 16, 15 and 15 eV for 028, 0,2, 10 and 0,2, 12 reflections. These values of V_{or} do not appear to be kinematically interpretable and require a full dynamical treatment which will be described in a subsequent paper.

Inspection of the reflectivities shown in figure 9 reveals that the $\phi = 0°$ azimuth gave consistently lower values than the $\phi = 45°$ azimuth. This is the case for all the data taken. An explanation has been sought in terms of experimental difficulties of one kind and another but no such interpretation has been found. Nevertheless, the intensity scales in figures 8–11 should be treated as arbitrary for the time being.

Acknowledgments

The authors would like to thank Dr A Chambers for useful discussions about photometer scanning arrangements and Mr J C Dee, Mr C Ovenden and Mr L Crosby for their help with construction of the cleavage manipulator and photometer mounts. We are grateful for the support of the Science Research Council.

References

Andersson S and Pendry J B 1972 *J. Phys.* C: *Solid St. Phys.* **5** 41
——1973 *J. Phys.* C: *Solid St. Phys.* **6** 601
Benson C G and Claxton T A 1968 *J. Chem. Phys.* **48** 1356
Demuth J E, Jepsen D W and Marcus P M 1973 *Phys. Rev. Lett.* **31** 540
Gallon T E, Higginbotham I G, Prutton M and Tokutaka H 1970 *Surface Sci.* **21** 224, 233 and 241
Janssen A P, Schoonmaker R C, Chambers A and Prutton M 1974 *Surface Sci.* **45** 45
Jepsen D W, Marcus P M and Jona F 1972 *Phys. Rev.* B **5** 3933
Jona F 1970 *IBM J. Res. Dev.* **14** 444
Laramore G E and Switendick A C 1972 *Phys. Rev.* B **7** 3615
Lord D G and Gallon T E 1973 *Surface Sci.* **36** 606
McRae E G and Caldwell C W Jr 1967 *Surface Sci.* **7** 41
Palmberg P W, Todd C J and Rhodin T N 1968 *J. Appl. Phys.* **39** 4650
Whetten N R and Laponsky A B 1957 *Phys. Rev.* **107** 1521